NACA RM L50J03

NACA

RESEARCH MEMORANDUM

AN INVESTIGATION OF THE LONGITUDINAL CHARACTERISTICS OF THE X-3 CONFIGURATION USING ROCKET-PROPELLED MODELS

PRELIMINARY RESULTS AT MACH NUMBERS FROM 0.65 TO 1.25

By Jesse L. Mitchell and Robert F. Peck

Langley Aeronautical Laboratory
Langley Air Force Base, Va.

NATIONAL ADVISORY COMMITTEE
FOR AERONAUTICS

WASHINGTON

December 1, 1950
Declassified October 14, 1957

NACA RM L50J03

NATIONAL ADVISORY COMMITTEE FOR AERONAUTICS

RESEARCH MEMORANDUM

AN INVESTIGATION OF THE LONGITUDINAL CHARACTERISTICS OF THE X-3 CONFIGURATION USING ROCKET-PROPELLED MODELS

PRELIMINARY RESULTS AT MACH NUMBERS FROM 0.65 TO 1.25

By Jesse L. Mitchell and Robert F. Peck

SUMMARY

A rocket-propelled model of the X-3 configuration has been flown through the Mach number range from 0.65 to 1.25. An analysis of the response of the model to rapid deflections of the horizontal tail gave information on the lift, drag, longitudinal stability and control, and longitudinal-trim change. The lift-coefficient range covered by the test was from -0.2 to 0.3 throughout most of the Mach number range.

The model was statically and dynamically stable throughout the lift-coefficient and Mach number range of the test. At subsonic speeds the aerodynamic center moved forward with increasing lift coefficient. The most forward position of the aerodynamic center was about 12.5 percent of the mean aerodynamic chord at a small positive lift coefficient and at a Mach number of about 0.84. At supersonic speeds the aerodynamic center was well aft, varying from 33 to 39 percent of the mean aerodynamic chord at Mach numbers of 1.0 and 1.25, respectively.

Transonic-trim change, as measured by the change in trim lift coefficient with Mach number at a constant tail setting, was of small magnitude (about 0.1 lift coefficient for zero tail setting).

The zero lift-drag coefficient increased about 0.042 in the region between a Mach number of 0.9 and 1.1.

INTRODUCTION

The National Advisory Committee for Aeronautics has initiated a test program employing free-flight rocket-propelled models for the purpose of evaluating the longitudinal stability and control characteristics and the external drag of the X-3 configuration at transonic and supersonic speeds. The first of these test vehicles was a fixed-control configuration designed to obtain longitudinal-trim and booster-separation characteristics. The results of the flight test of the second model which employed an all-movable horizontal tail are given in this paper.

The longitudinal aerodynamic characteristics of the test vehicle were obtained from measurements made during the free-pitching oscillations following abrupt changes in the incidence of the all-movable horizontal tail. The Mach number range investigated was from 0.65 to 1.25. The model was flown at the Langley Pilotless Aircraft Research Station, Wallops Island, Va.

SYMBOLS

C_N	normal-force coefficient $\left(\frac{a_n W}{gSq}\right)$
C_C	chord-force coefficient $\left(\frac{-a_l W}{gSq}\right)$
C_D	drag coefficient $\left(C_C \cos \alpha + C_N \sin \alpha\right)$
C_L	lift coefficient $\left(C_N \cos \alpha - C_C \sin \alpha\right)$
C_m	pitching-moment coefficient
a_n/g	normal accelerometer reading
a_l/g	longitudinal accelerometer reading
W	weight, pounds
S	wing area (including area enclosed within fuselage), square feet
q	dynamic pressure, pounds per square foot

α angle of attack, degrees

G torsional modulus of elasticity, pounds per square inch

c_t tip chord of wing, inches

m_θ wing torsional stiffness parameter, inch pounds per radian

m couple applied near wing tip in plane parallel to model center line and normal to chord plane, inch-pounds

θ local wing twisting angle produced by m measured in plane parallel to model center line and normal to chord plane, radians

θ angle of pitch, degrees

y lateral distance from side of fuselage, inches

$b_e/2$ exposed wing semispan (measured from side of fuselage), inches

R Reynolds number based on wing mean aerodynamic chord

M Mach number

δ horizontal tail deflection, degrees

t time, seconds

$t_{1/2}$ time to damp to one-half amplitude, seconds

C_n yawing-moment coefficient

β sideslip angle, degrees

$\bar{c}$ mean aerodynamic chord, feet

V velocity, feet per second

l_t tail length, feet

Subscripts:

$\dot{\alpha}$ $\frac{d\alpha}{dt}\frac{\bar{c}}{2V}$, degrees

q $\frac{d\theta}{dt}\frac{\bar{c}}{2V}$, degrees

The symbols α, δ, q, $\dot{\alpha}$, and β used as subscripts indicate the derivative of the quantity with respect to the subscript, for example

$$C_{N_\alpha} = \frac{\partial C_N}{\partial \alpha}$$

MODEL AND APPARATUS

The X-3 configuration tested had a slender fuselage with dual air inlets located near the top of the fuselage and a 4.5-percent-thick straight wing of aspect ratio 3.0 and taper ratio 0.4. The horizontal and vertical tail were mounted on a boom behind the fuselage. Details of the model are shown in figures 1, 2, and 3. A Deacon rocket booster (fig. 4) propelled the model to a maximum Mach number of 1.32; however, due to the time required for separation of the model from the booster, model-alone data were obtained only up to a Mach number of 1.25.

In order that the external flow conditions about the model be approximately correct, a simple air-induction system was incorporated in the model to give approximately the correct mass flow through the inlets. These inlets (see fig. 5) were connected to constant-diameter ducts designed for choked flow at the exits.

The model was of all-metal construction. The body was formed from magnesium castings and dural sheet while the wings and tail surfaces were made from solid dural. The type of construction used resulted in a comparatively rigid structure. For purposes of future comparison with other data the wing torsional stiffness is given in figure 6.

A hydraulic accumulator provided power to pulse the horizontal tail in a predetermined pattern during the coasting part of the flight. A seven-channel NACA telemeter transmitted continuous information on free-stream total pressure, normal acceleration, longitudinal acceleration, angle of attack, and horizontal tail position; plus intermittent data on transverse acceleration, and a calibrated static pressure. The Doppler velocimeter, SCR 584 flight-path radar, and radiosonde were used to check the free-stream conditions at the model during part of its flight.

The weight of the model was 137.8 pounds and the center of gravity was 15 percent ahead of the leading edge of the mean aerodynamic chord. The moment of inertia of the model in pitch was 17.1 slug-feet square.

The Reynolds number of the test (based on the mean aerodynamic chord) is shown in figure 7.

TEST AND ANALYSIS PROCEDURES

The test technique employed in obtaining these data was that of disturbing the model in pitch by means of an all-movable horizontal tail while the model decelerated through the Mach number range. The response of the model to the disturbance was measured by means of instruments in the model and transmitted to the ground by means of a telemeter.

The basic data obtained were time histories of free-stream total pressure, static pressure, and temperature; three components of acceleration; angle of attack; and control position. From these basic data were obtained time histories of Mach number, velocity, dynamic pressure, Reynolds number, normal-force coefficient, chord-force coefficient, angle of attack, control position, periods of the oscillations due to the control disturbance, and time for the oscillation to damp to one-half amplitude.

These data were then analyzed by the methods discussed in reference 1 to obtain the variation with Mach number of longitudinal stability, control, trim, and drag of the configuration.

ACCURACY AND CORRECTIONS

Accuracy

From a consideration of possible zero shifts in the telemetered data of 1 to 2 percent of the full-scale instrument range, and on the basis of limited independent checks of the Mach number and static pressure, the limits of accuracy of some of the important quantities obtained from the flight-test data are believed to be as follows:

	M = 1.25	1.00	0.80	0.65
C_N	±0.014	±0.024	±0.041	±0.070
C_C	±0.0014	±0.0024	±0.0041	±0.007
α	±0.3 deg	±0.3 deg	±0.3 deg	±0.3 deg
δ	±0.15 deg	±0.15 deg	±0.15 deg	±0.15 deg
M	±0.01	±0.01	±0.015	±0.02

In addition the absolute angle of attack may be further in error due to undetermined aerodynamic zero shifts of the free-floating vane used to measure the angle of attack.

The aforementioned errors are systematic, that is, they always tend to either increase or decrease the measured quantities over the Mach number range investigated. Consequently, these errors have only minor effects on both the trends indicated by the measurements and on slopes and incremental quantities derived from the measurements.

Corrections

The indicated angle of attack, normal acceleration, and longitudinal acceleration have been corrected for position error since none of these instruments was located at the center of gravity. The angle-of-attack corrections were made as described in reference 2 and the accelerometer corrections were made from a consideration of the equations of motion to obtain pitching velocity and acceleration.

DISCUSSION

Time Histories

As pointed out in a previous section, the data were obtained as time histories. A typical response of the model to a control movement is shown in figure 8. Note the pitch oscillation induced by the control movement.

Lift

Inasmuch as the maximum difference between normal-force coefficient and lift coefficient for these tests is only of the order of 1 percent, the values of lift coefficient were taken equal to the normal-force coefficient. Figure 9 presents lift coefficient against angle of attack for various Mach numbers.

These data were obtained over one-half-to-one cycle of oscillation so that the Mach number change is small and the average Mach number can be used. (The maximum deviation from the average Mach number is ± 0.02 at a Mach number of 1.25.) In general, different values of angle of attack, for a given value of lift coefficient, were obtained, depending on whether the angle of attack was increasing or decreasing with time. This is evident in figure 9 in the form of a loop in the data. Part of this loop can be explained from aerodynamic considerations. For instance, it is known that a lift arises from the rate of change of angle of attack with time, so that it is not strictly correct to cross plot the time histories assuming lift proportional only to angle of attack. It is believed that this hysteresis does not affect the slopes of the curves.

From figure 9 it can be seen that the variation of lift with angle of attack is slightly nonlinear. These data are not complete enough to establish the exact variation of lift-curve slope with lift coefficient and Mach number. The variation of an average lift-curve slope with Mach number is shown in figure 10.

Drag

The drag coefficients were computed from C_N, C_C, and α. Figure 11 gives the variation of drag coefficient with Mach number for various lift coefficients.

These drag data are total measured drag and include the drag due to the air-induction system. The external drag can only be obtained approximately since not enough telemeter channels were available on this model to measure the internal drag. Estimations of the internal drag coefficient, at Mach numbers of 0.8 and above, have been made. These calculations assumed that the design criteria of the system, that is, mass-flow ratios of about 0.8 and choked flow at the exit were met. The values of the estimated internal drag coefficients are also given in figure 11.

The transonic drag rise occurred at approximately 0.9 Mach number and the drag coefficient increase at zero lift was about 0.042. Note in figure 11 also that in the region from 0.7 to 0.85 there is an evident decrease in drag at constant lift coefficients. This is at least qualitative evidence that the induced drag coefficient varies inversely with the lift-curve slope. Insufficient data preclude the determination of a quantitative measurement of the law of variation of induced drag for this configuration.

Longitudinal Stability

Static stability.- An analysis of the oscillations in pitch induced by the control movement indicates that the model is statically and dynamically stable in the speed range and lift-coefficient range covered by the test. Figure 12(a) presents the periods of the oscillations from which the static-stability parameter C_{m_α} (fig. 12(b)) was calculated. A somewhat more useful picture of the stability may be obtained by dividing C_{m_α} by C_{L_α} and converting to aerodynamic-center location. Figure 12(c) is a plot of aerodynamic-center position for this model. The aerodynamic center moves forward with increasing lift coefficient at subsonic speeds. The most forward position is about 12.5 percent of the mean aerodynamic chord at a small positive lift coefficient and at a Mach number of about 0.84. The aerodynamic center is well aft at supersonic

speeds varying from 33 to 39 percent of the mean aerodynamic chord at Mach numbers of 1.0 and 1.25, respectively.

Damping in pitch.- Damping in pitch as determined from the rate of decay of the oscillations in pitch is shown in figure 13. One curve was faired through the measured time to damp to one-half amplitude (fig. 13(a)) since no definite difference is evident in this quantity for the two lift-coefficient ranges. The values of the damping factor $C_{m_q} + C_{m_{\dot{\alpha}}}$ are shown in figure 13(b). This quantity also varies slightly with lift coefficient as might be expected since the lift is slightly nonlinear (fig. 9). The values of the damping derivative are about the order of magnitude that would be expected by assuming that the horizontal tail contributes the major portion of the damping. The increase in the damping factor near a Mach number of 1.0 is indicated by other tests (reference 3) and is probably associated with a corresponding increase in tail lift-curve slope in this region.

Trim and Control

The variation with Mach number of trim angle of attack and lift coefficient for two horizontal tail deflections is shown in figure 14 (the word "trim" used in connection with these data refers to the condition of zero pitching moment). The solid lines indicate where the data were obtained alternately at the two tail settings and the dotted lines are faired on the basis of other data from a fixed-control model. Figure 14 indicates a small trim change through the transonic region.

An average effectiveness of the horizontal tail in producing pitching moment C_{m_δ} and lift C_{L_δ} can be obtained by several methods from the data presented in this report. It is believed that the following expressions give the best estimate of these parameters for this model:

$$C_{m_\delta} \approx C_{m_\alpha}\left(\frac{\Delta\alpha}{\Delta\delta}\right)_{trim}$$

and

$$C_{L_\delta} \approx \frac{C_{m_\delta}}{l_t/\bar{c}}$$

The values obtained are shown in figure 15 as functions of Mach number.

Directional Stability

The lateral acceleration of the model was small throughout the Mach number range of the tests, never being larger than about 0.25g. There was a small-amplitude lateral oscillation, however, and the periods of this oscillation varied as shown in figure 16(a). Assuming that these periods were proportional to the directional stability as in reference 3, the parameter C_{n_β} was calculated (see fig. 16(b)). For these calculations the reasonable assumption was made that the moment of inertia in yaw was equal to the moment of inertia in pitch.

Comparison with Wind-Tunnel Results

A comparison of some of the rocket test results with the wind-tunnel results of reference 4 is shown in figure 17. The wind-tunnel data were obtained on a model of an early version of the X-3 which had a relatively shorter and less voluminous nose than the rocket model. In addition, the wind-tunnel model had no air flow through the inlets, whereas the rocket model had open inlets with air flow through the model exhausting at the rear of the fuselage forward of and below the horizontal tail.

In general, the agreement between the two tests is considered satisfactory. It should be noted that the lift-curve slope and tail lift effectiveness shown for the rocket model are average values of these quantities, whereas the comparative results for the wind-tunnel model are values measured at a particular lift coefficient or angle of attack. The more forward position of the aerodynamic center of the rocket model as compared to the wind-tunnel model is compatible with the differences between the two models. No explanation can be given at this time for the comparatively lower directional stability of the rocket model; however, the previously discussed differences between the two models plus small differences in boom and vertical-tail geometry may be contributing factors.

CONCLUSIONS

A rocket-propelled model of the X-3 with an all-movable tail has been flown. The pulsed control technique was used to obtain the longitudinal characteristics of the model in the lift-coefficient range from about -0.2 to 0.3 at Mach numbers from 0.65 to 1.25. The data obtained indicate the following conclusions:

1. The model was statically and dynamically stable throughout the lift-coefficient and Mach number range of the test. At subsonic speeds the aerodynamic center moved forward with increasing lift coefficient.

The most forward position of the aerodynamic center was about 12.5 percent of the mean aerodynamic chord at a small positive lift coefficient and at a Mach number of about 0.84. At supersonic speeds the aerodynamic center was well aft, varying from 33 to 39 percent of the mean aerodynamic chord at Mach numbers of 1.0 and 1.25, respectively.

2. The transonic trim change, as measured by the change in trim lift coefficient with Mach number at a constant tail setting, was of small magnitude (about $0.1C_L$ for $\delta = 0$).

3. The zero-lift drag rise began at about 0.9 Mach number, and the total increase in drag coefficient through the transonic region was about 0.042.

Langley Aeronautical Laboratory
National Advisory Committee for Aeronautics
Langley Air Force Base, Va.

REFERENCES

1. Gillis, Clarence L., Peck, Robert F., and Vitale, A. James: Preliminary Results from a Free-Flight Investigation at Transonic and Supersonic Speeds of the Longitudinal Stability and Control Characteristics of an Airplane Configuration with a Thin Straight Wing of Aspect Ratio 3. NACA RM L9K25a, 1950.

2. Mitchell, Jesse L., and Peck, Robert F.: An NACA Vane-Type Angle-of-Attack Indicator for Use at Subsonic and Supersonic Speeds. NACA RM L9F28a, 1949.

3. Bishop, Robert C., and Lomax, Harvard: A Simplified Method for Determining from Flight Data the Rate of Change of Yawing-Moment Coefficient with Sideslip. NACA TN 1076, 1946.

4. Hamilton, William T., and Cleary, Joseph W.: Wind-Tunnel Tests of a 0.16-Scale Model of the X-3 Airplane at High Subsonic Speeds.- Stability and Control Characteristics. NACA RM A50A03, 1950.

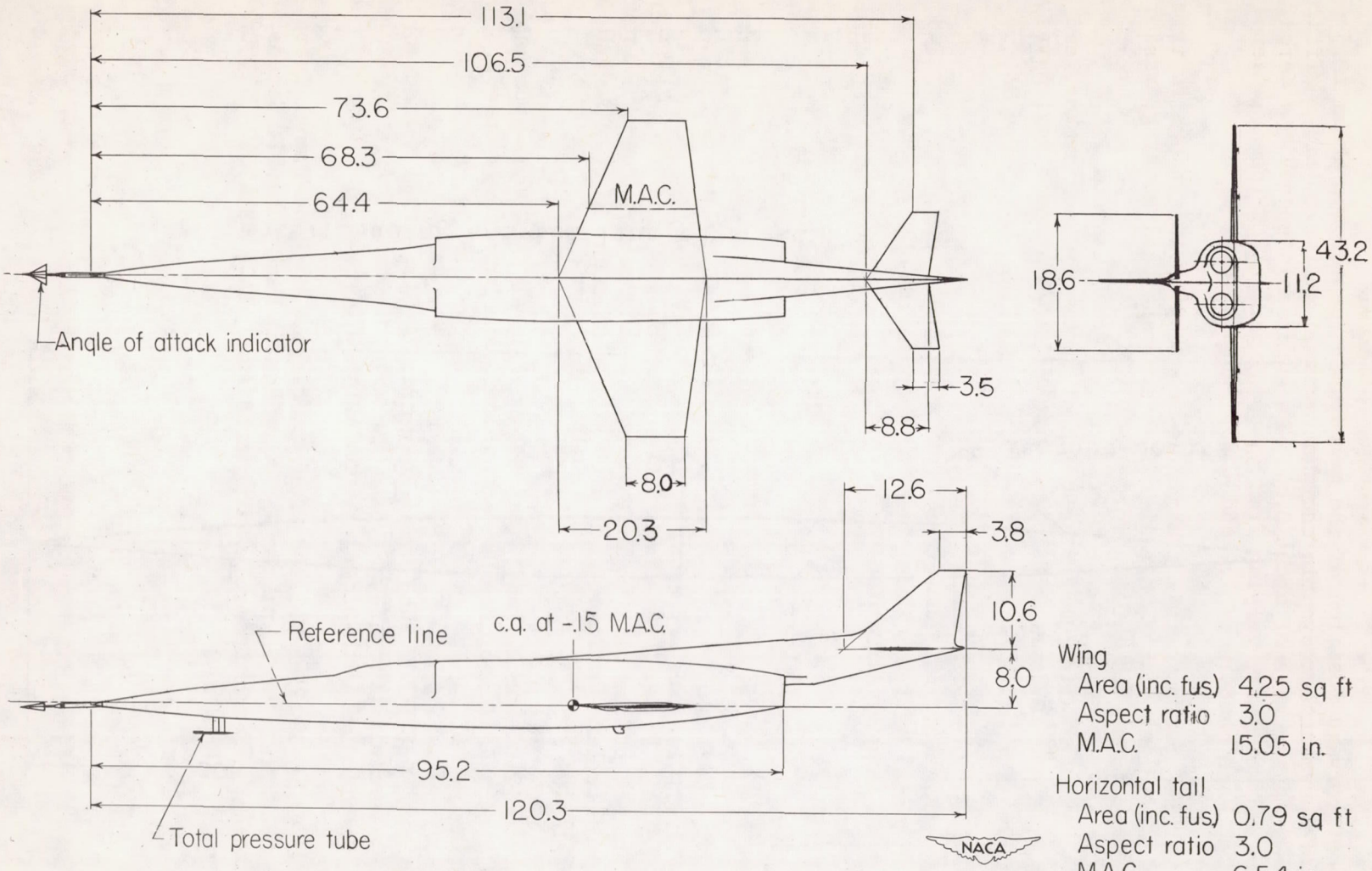

Wing

Area (inc. fus.)	4.25 sq ft
Aspect ratio	3.0
M.A.C.	15.05 in.

Horizontal tail

Area (inc. fus.)	0.79 sq ft
Aspect ratio	3.0
M.A.C.	6.54 in.

Figure 1.- General arrangement of X-3 model. All dimensions are in inches.

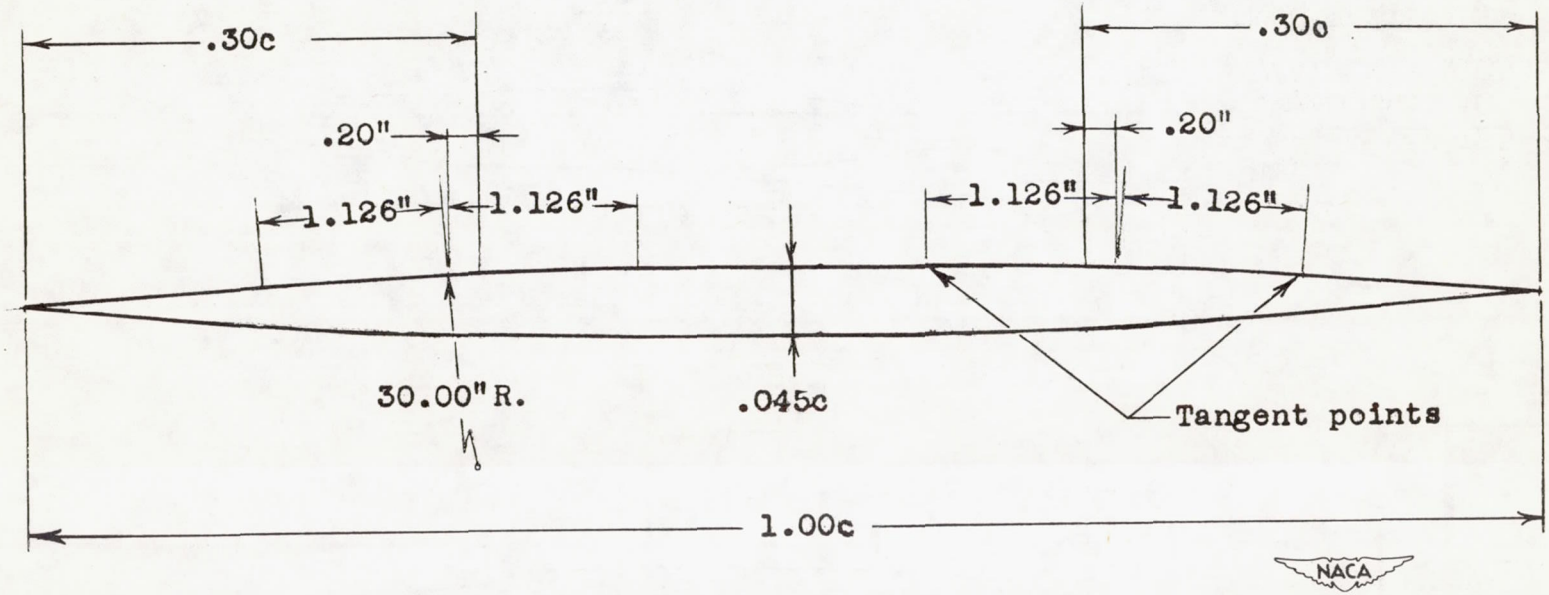

Note: Leading and trailing edge radii =0.015"

Figure 2.- Typical airfoil section of all surfaces on rocket-propelled X-3 model.

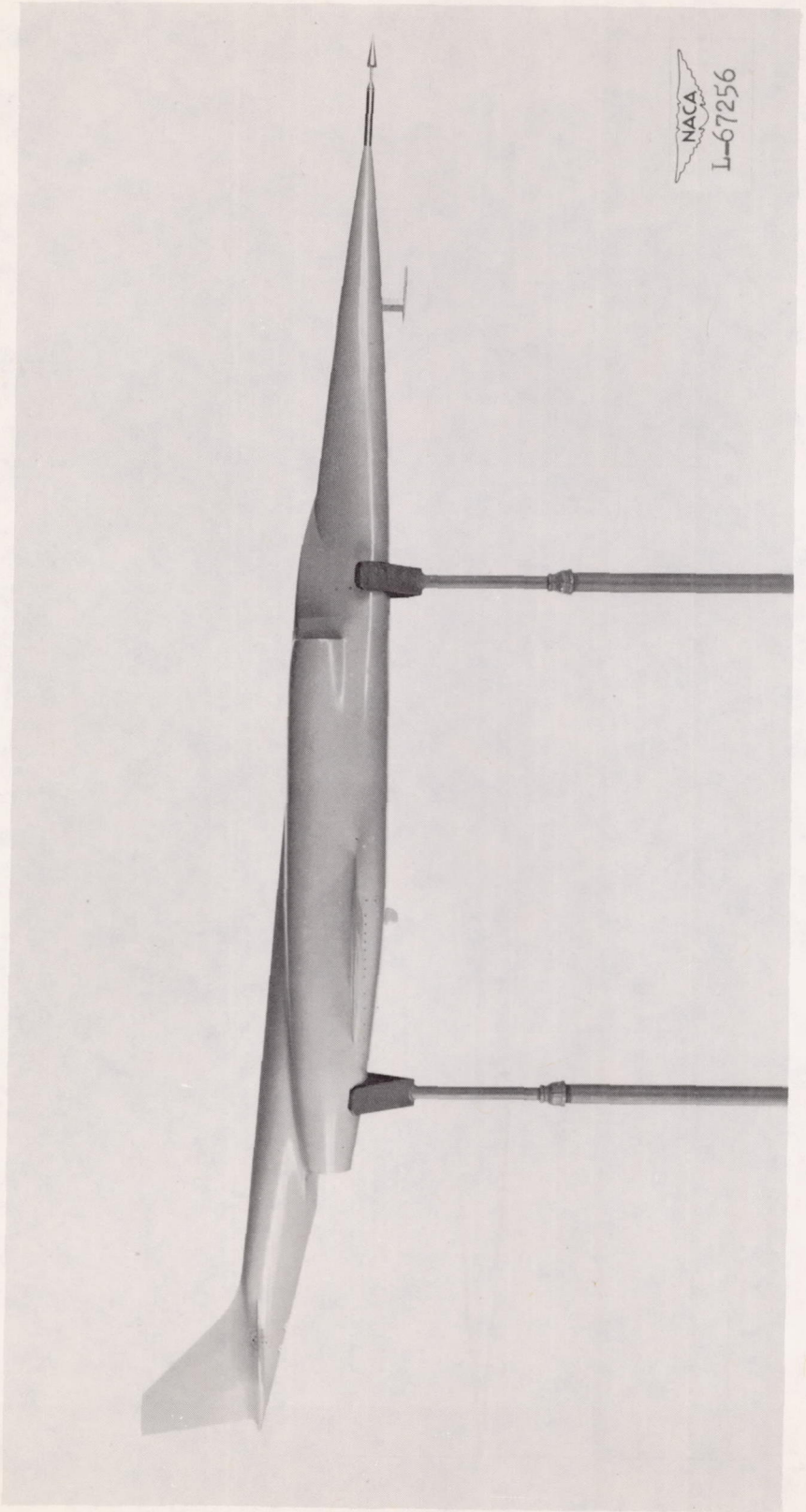

Figure 3.- Photographs of X-3 models.

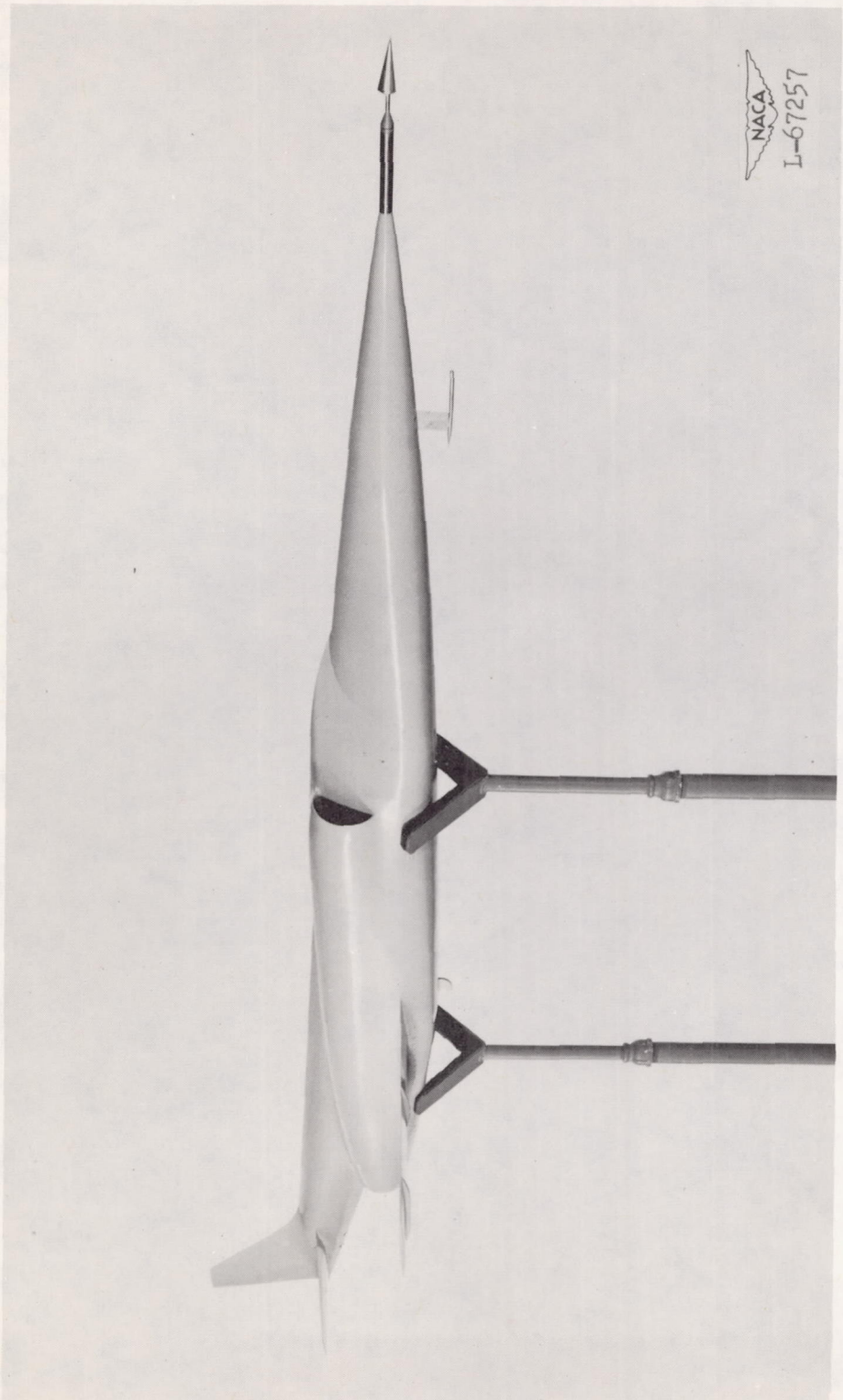

Figure 3.- Concluded.

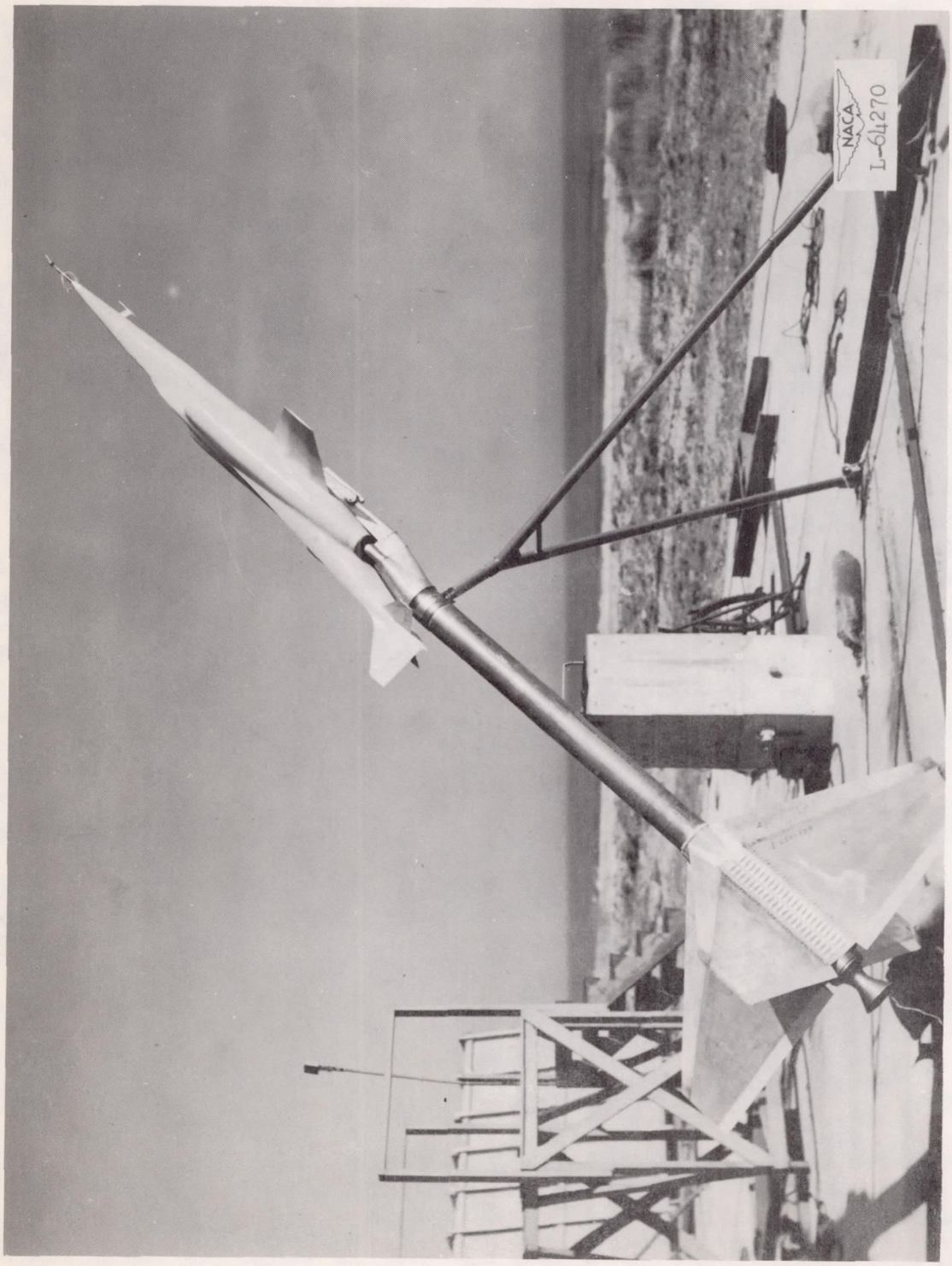

Figure 4.- Photograph of X-3 model on booster.

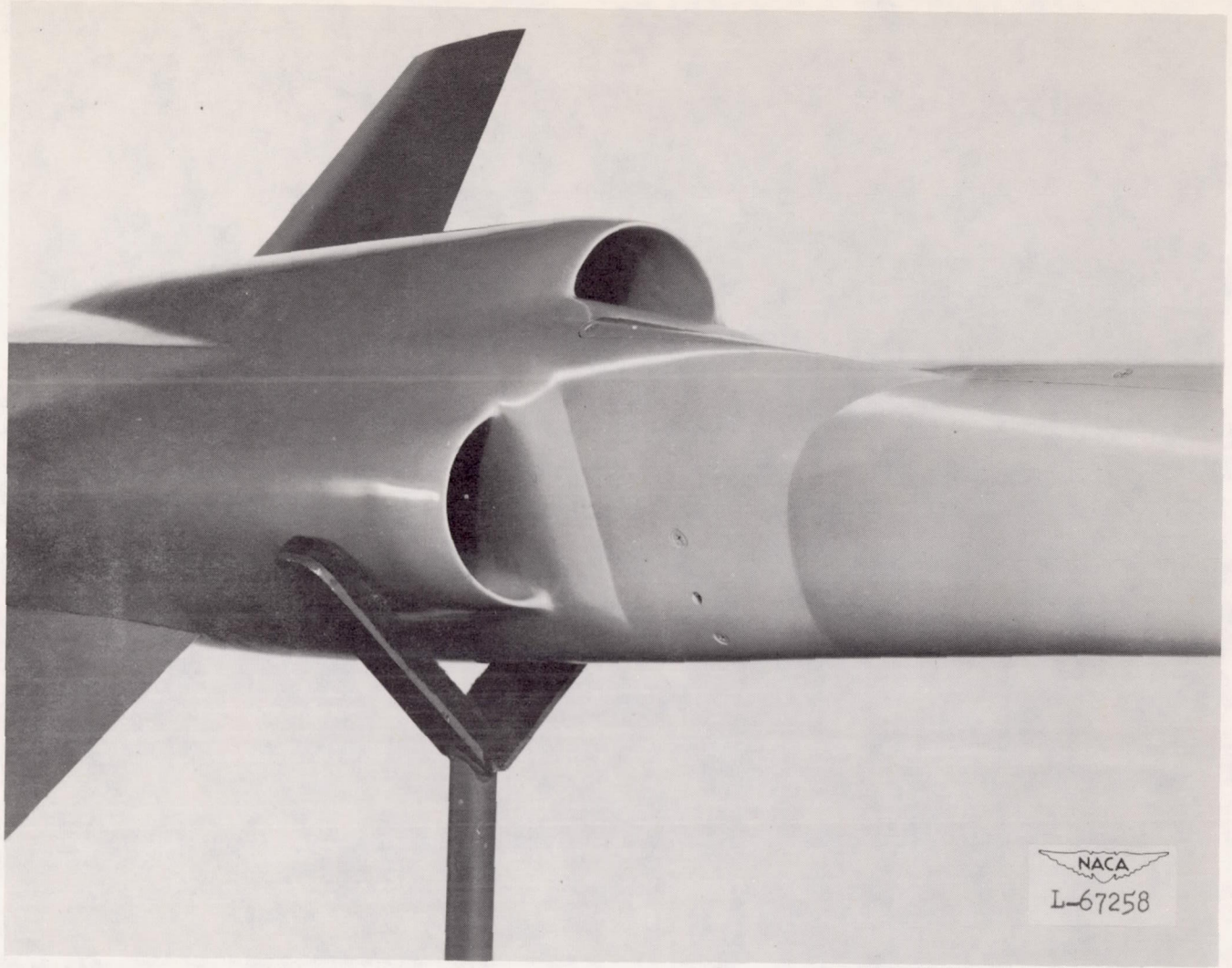

Figure 5.- Photograph of duct detail on X-3 model.

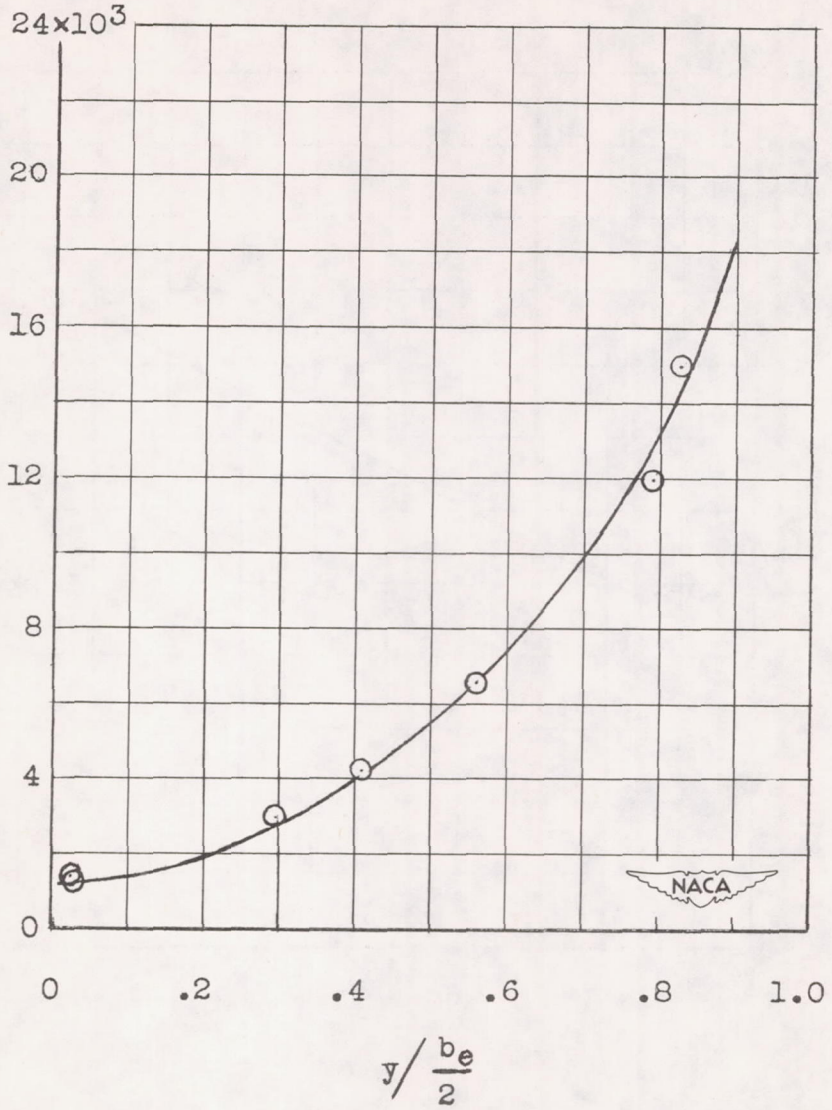

Figure 6.- Wing torsional stiffness parameter.

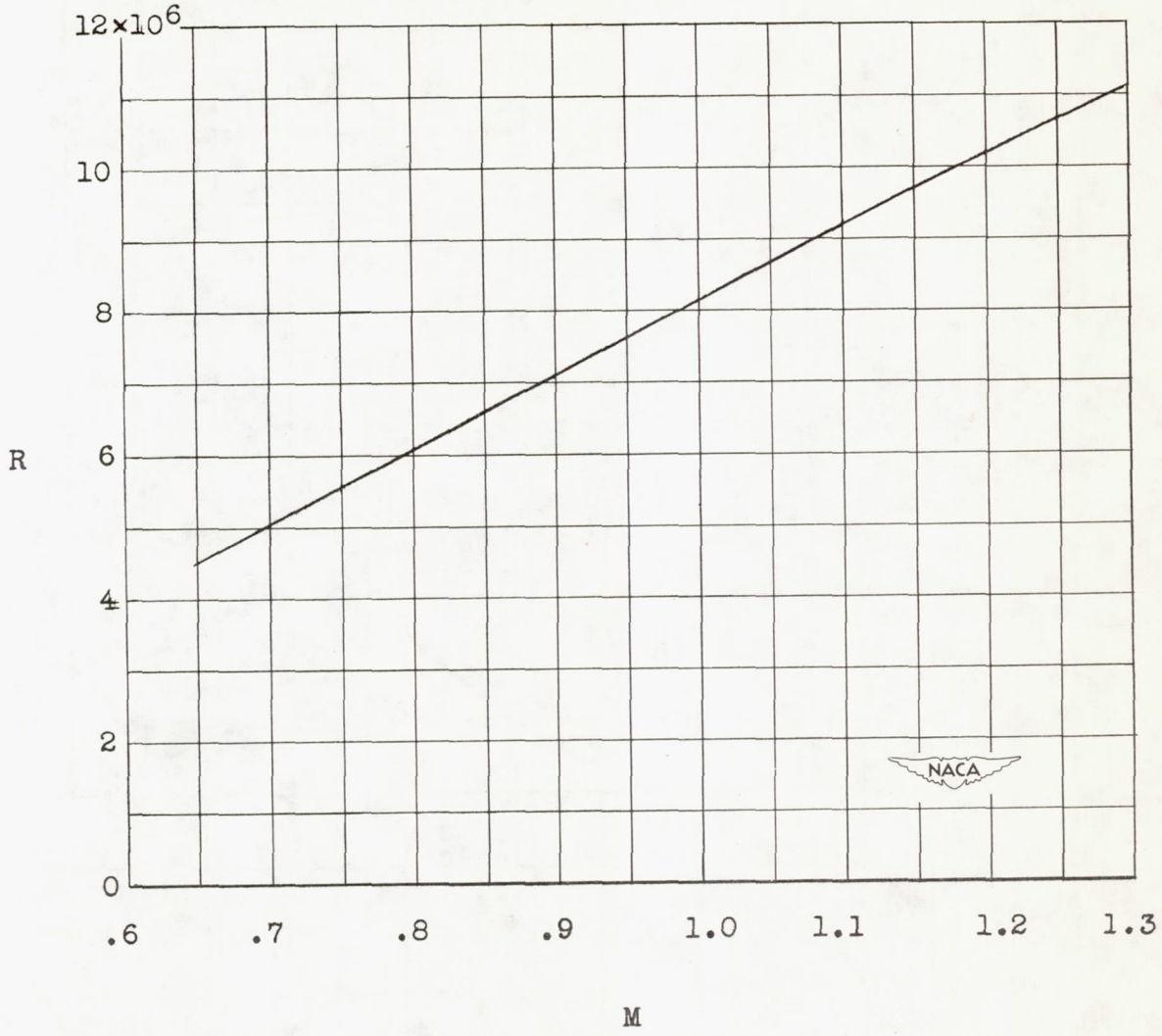

Figure 7.- Test Reynolds number based on mean aerodynamic chord.

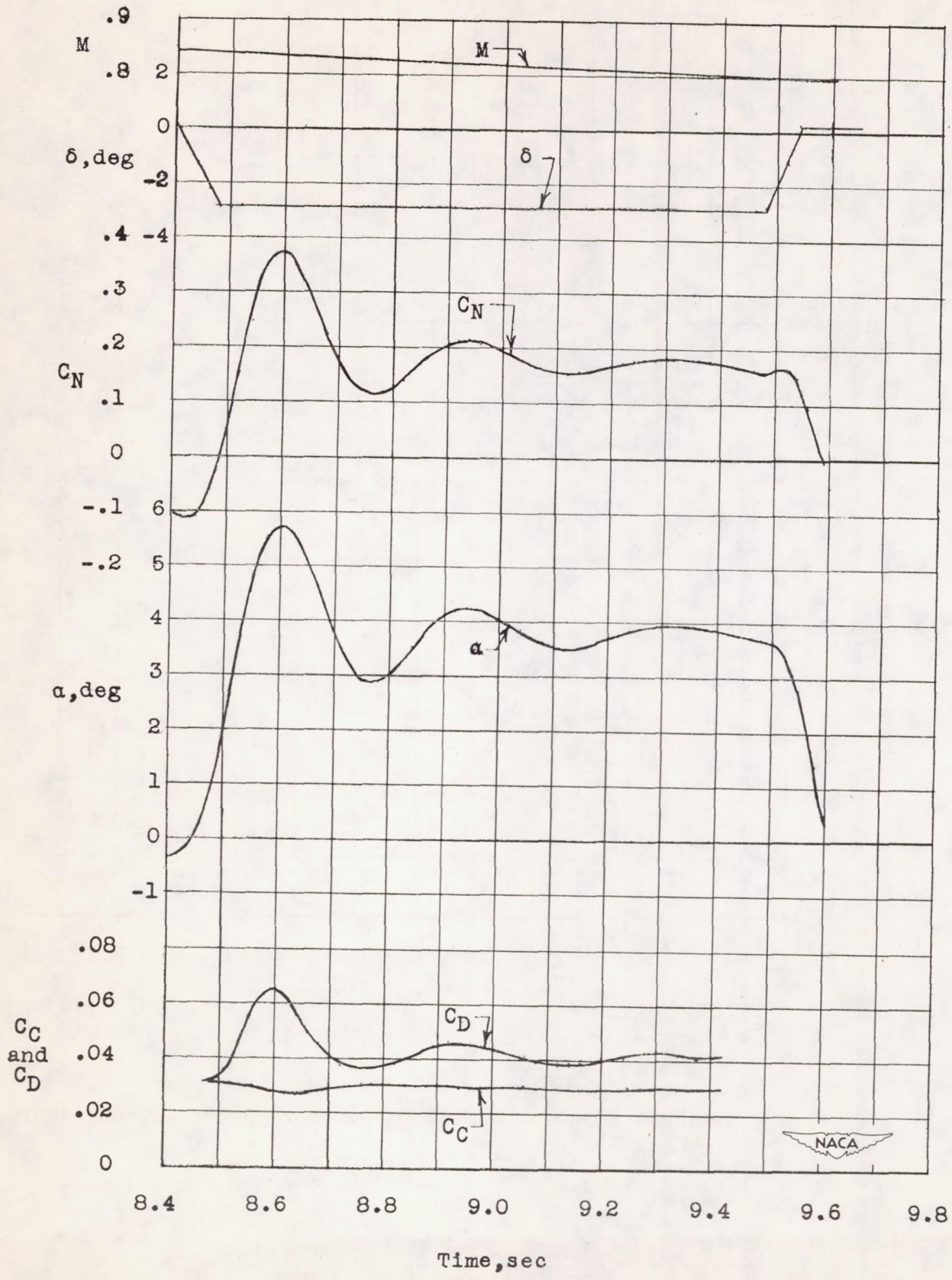

Figure 8.- Typical portion of time history.

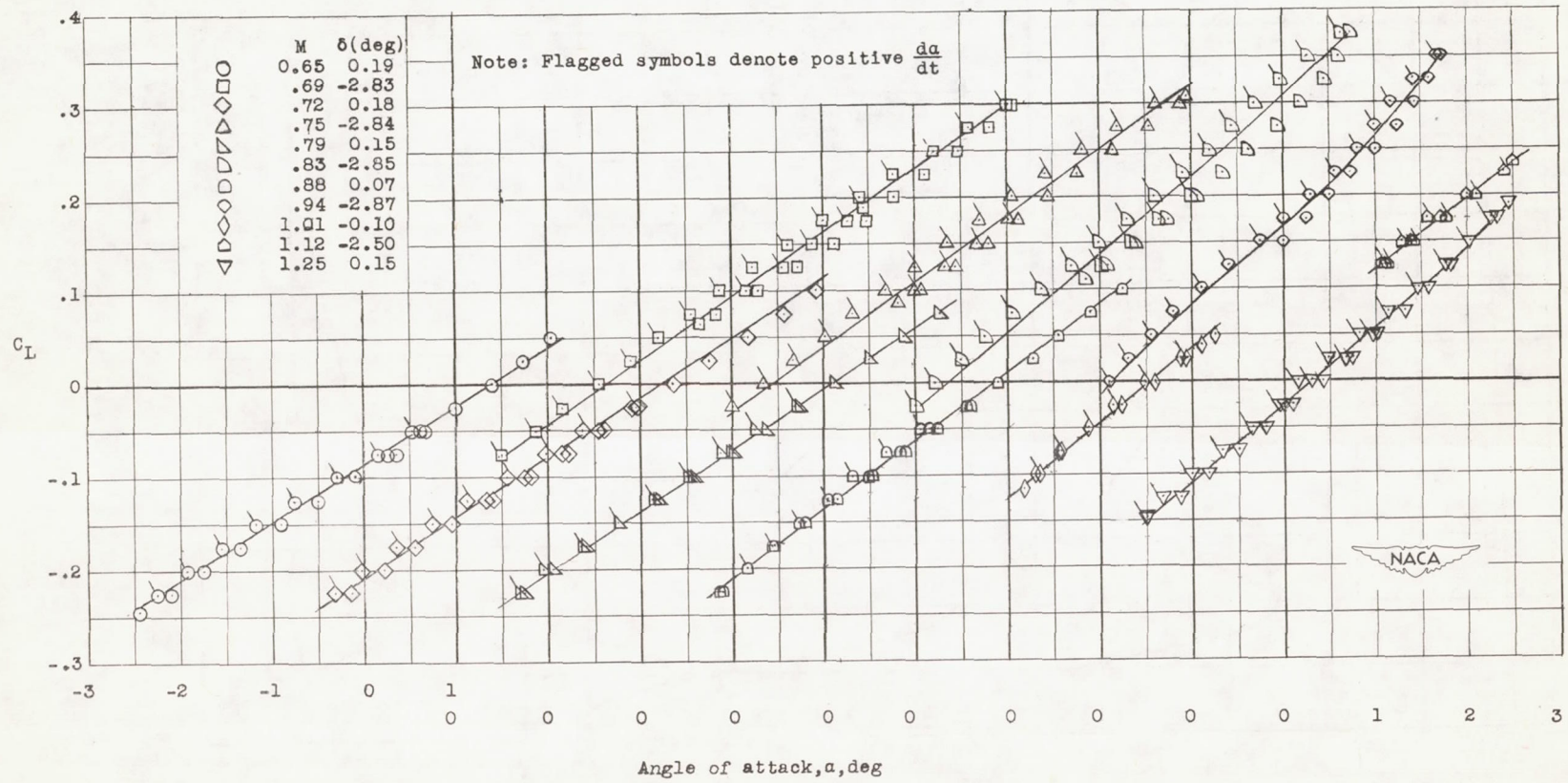

Figure 9.- Variation of lift coefficient with angle of attack.

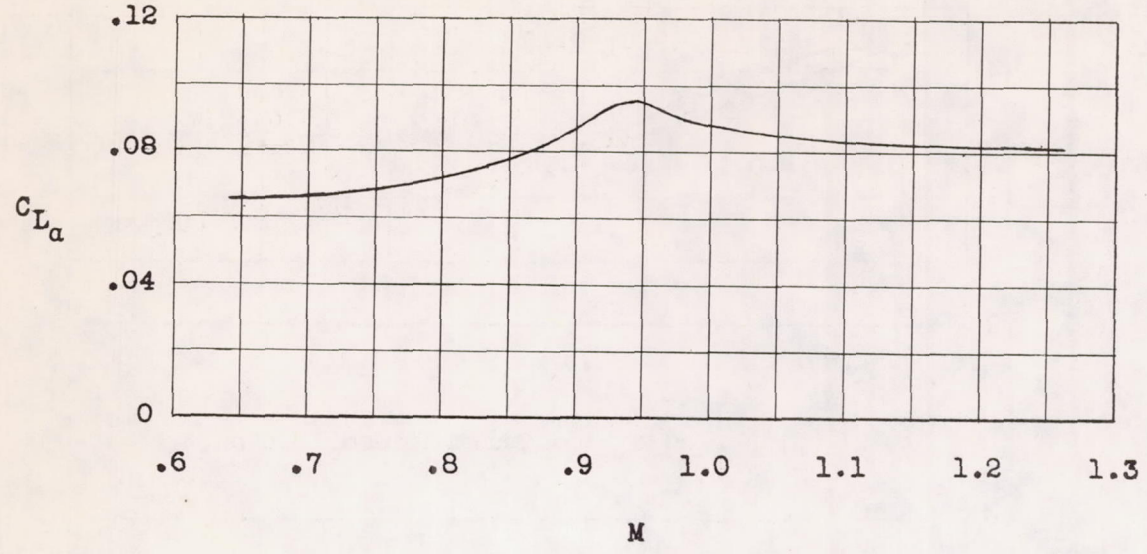

Figure 10.- Average lift-curve slope.

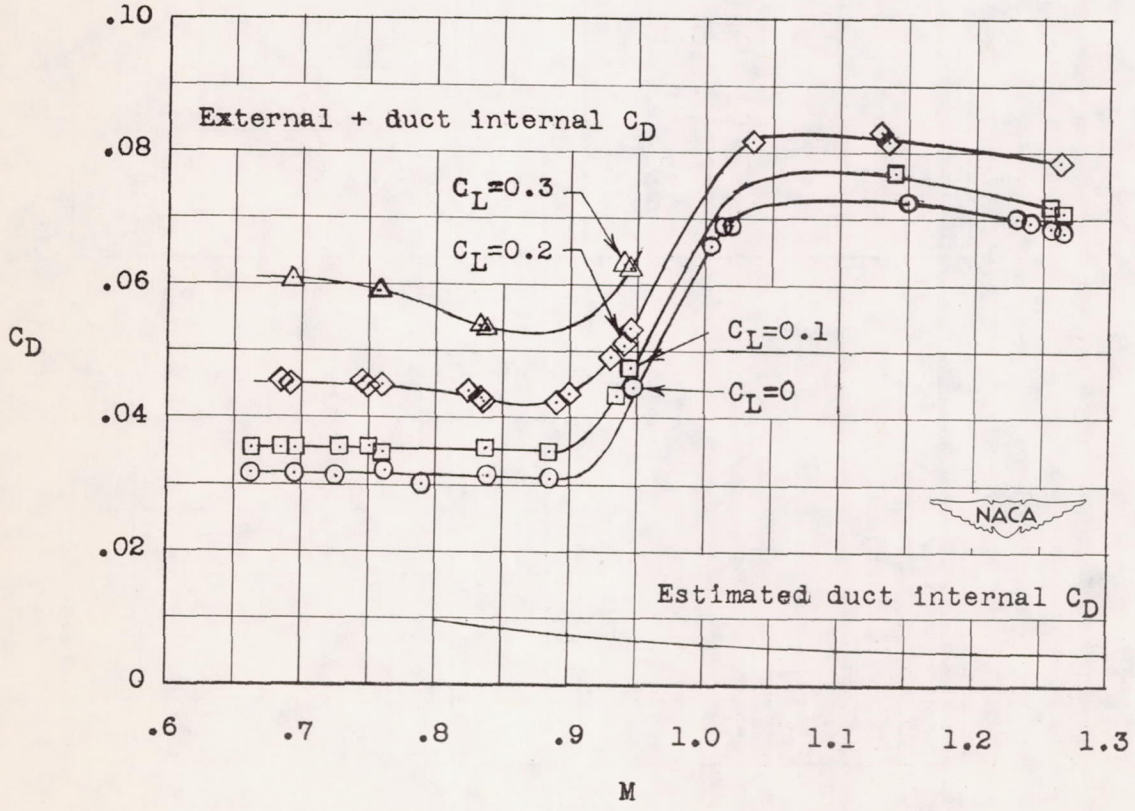

Figure 11.- Drag coefficients.

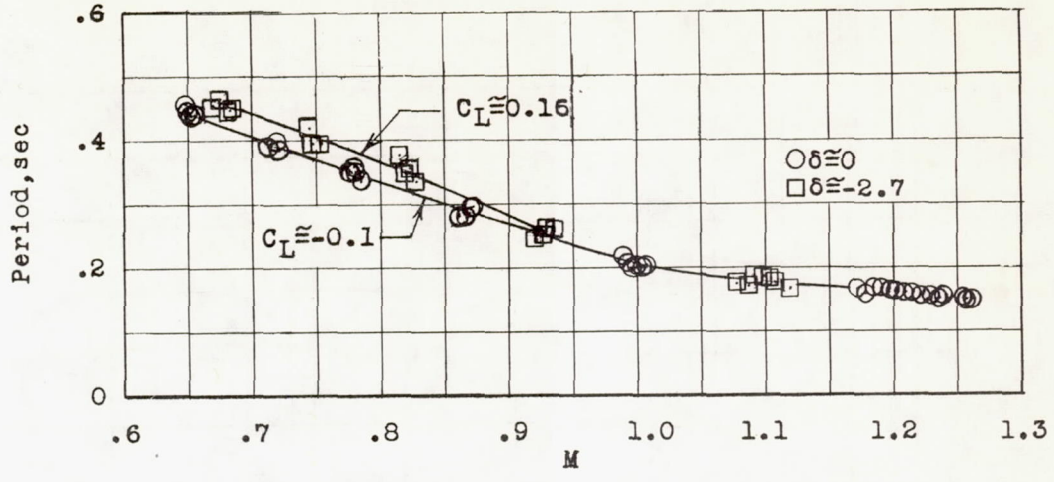

(a) Period of longitudinal oscillation.

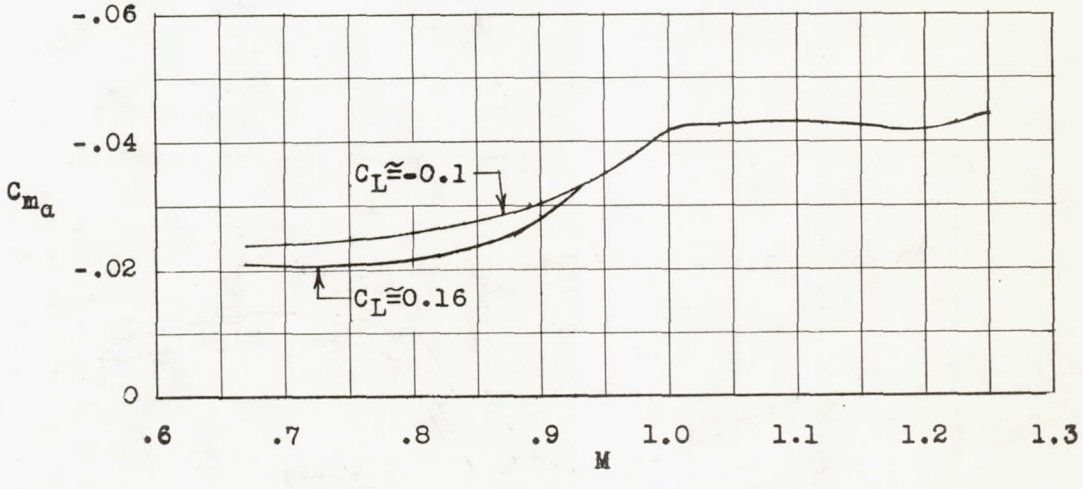

(b) Longitudinal stability parameter C_{m_α} with center of gravity at -15 percent M.A.C.

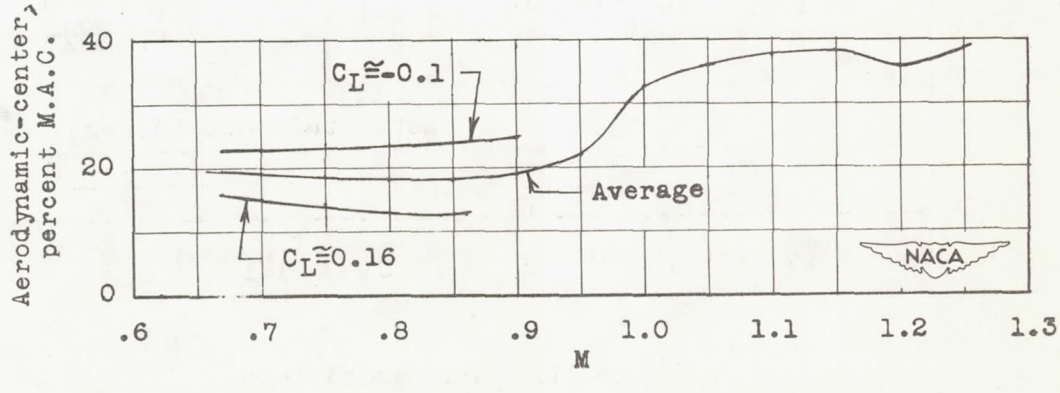

(c) Aerodynamic-center location.

Figure 12.- Static longitudinal stability characteristics.

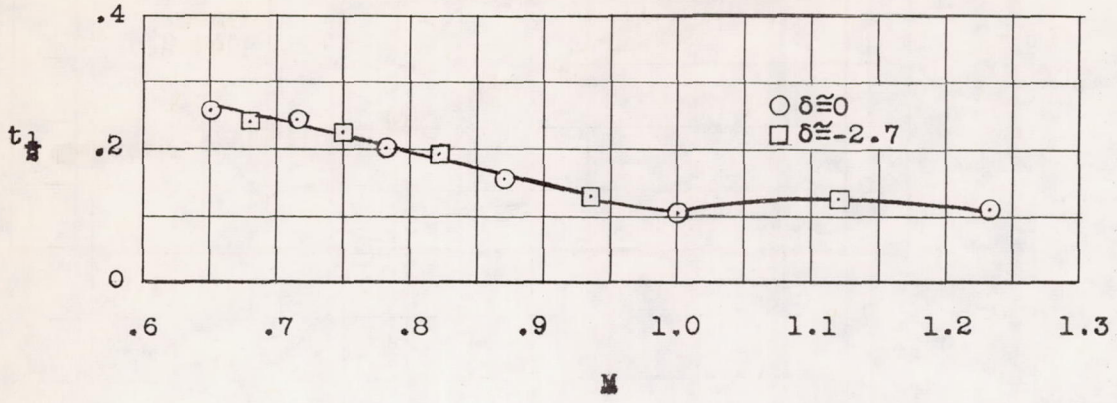

(a) Time to damp to one-half amplitude.

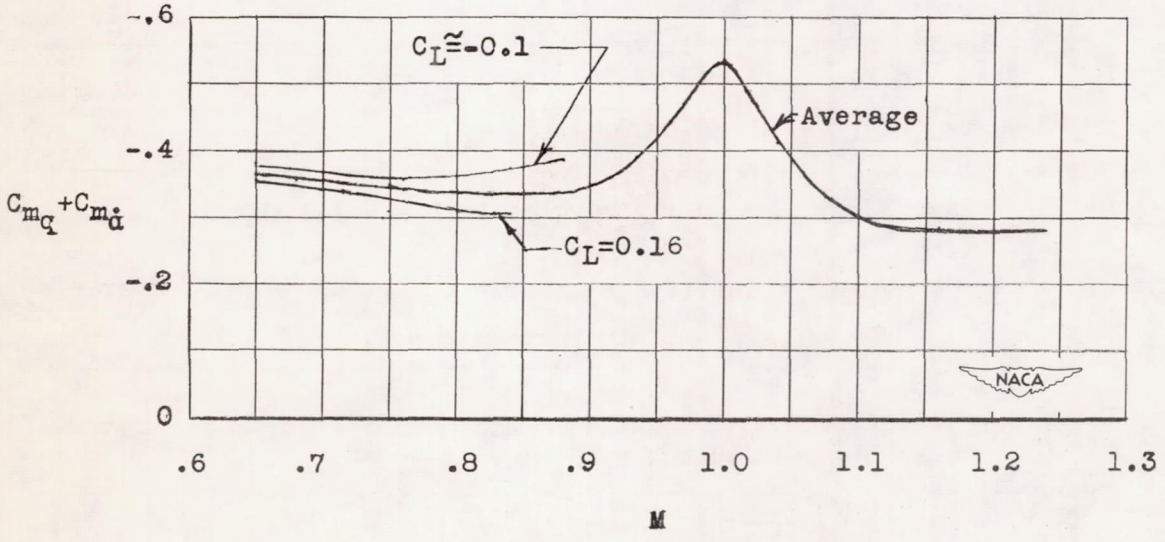

(b) Damping factor.

Figure 13.- Damping characteristics of longitudinal short-period oscillation.

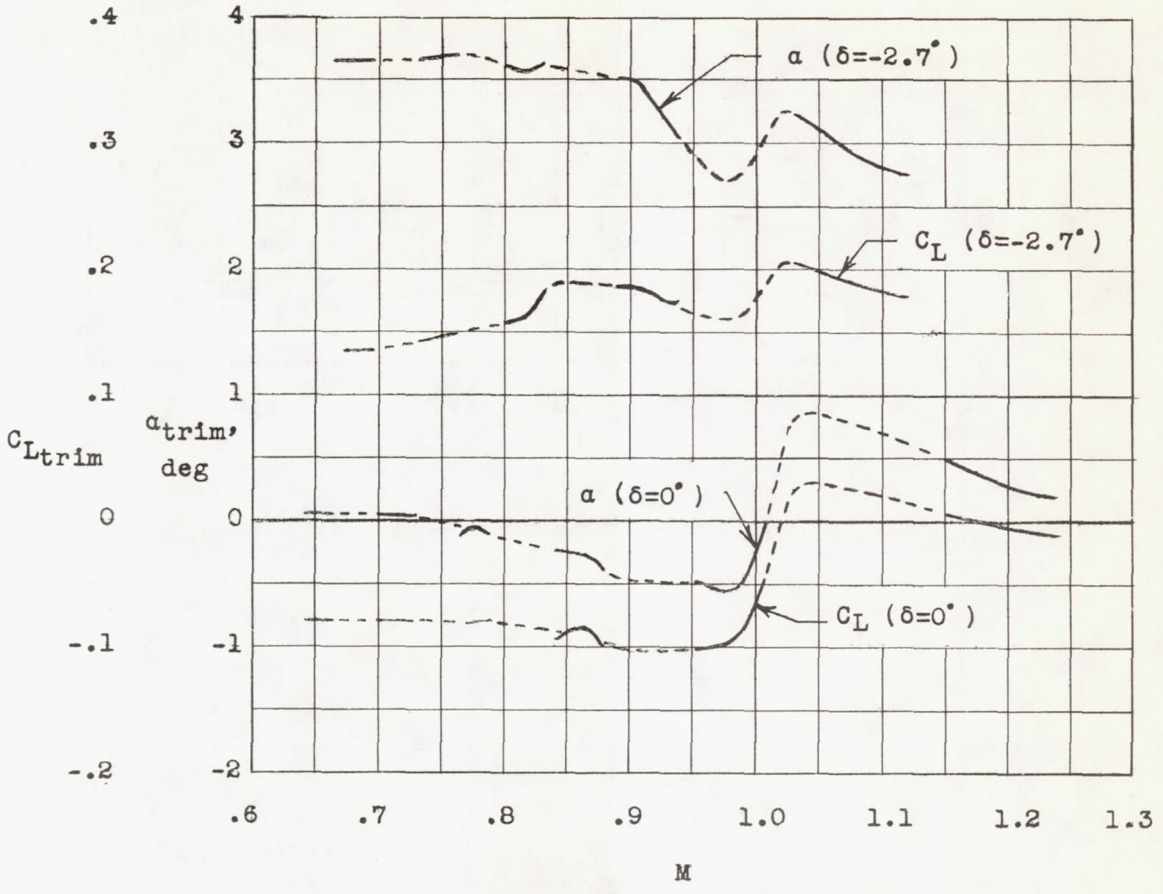

Figure 14.- Trim lift coefficient and angle of attack.

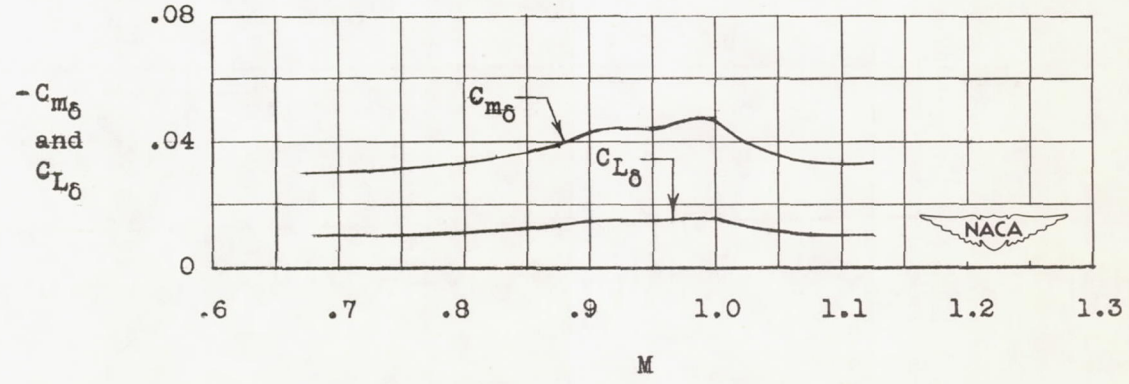

Figure 15.- Horizontal-tail effectiveness.

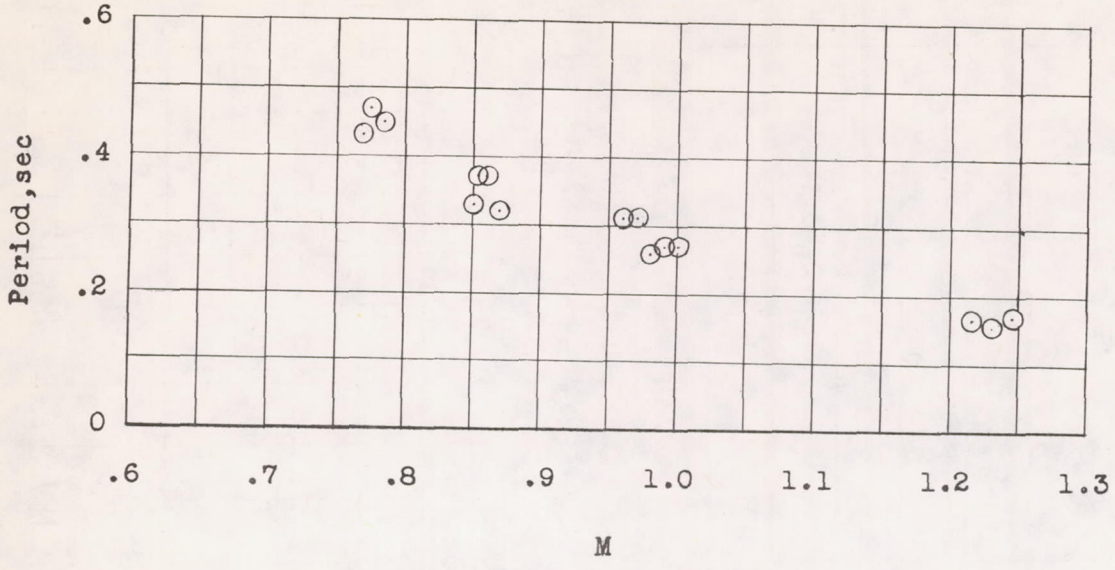

(a) Period of lateral oscillation.

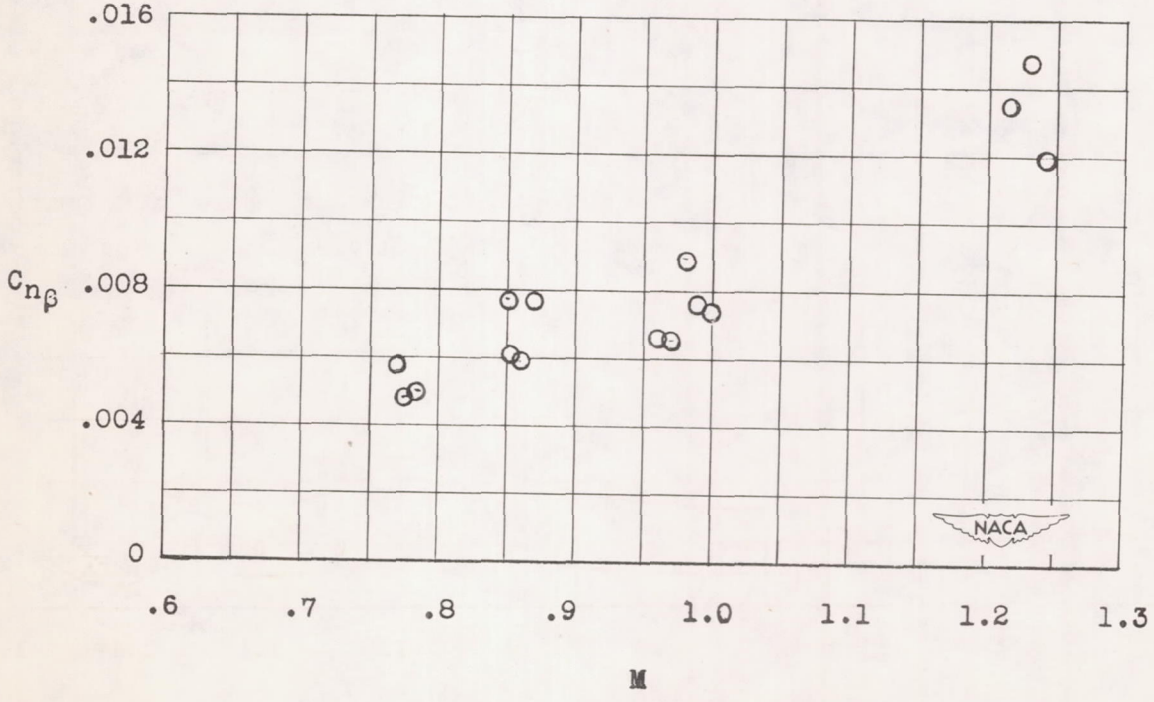

(b) Directional stability parameter.

Figure 16.- Directional stability.

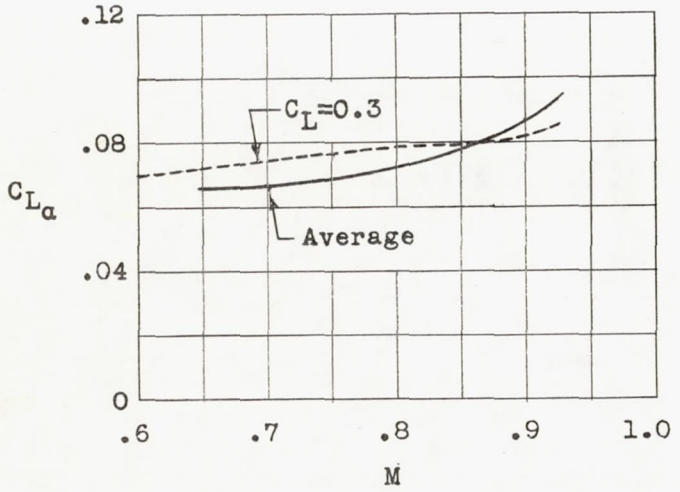

(a) Lift-curve slope.

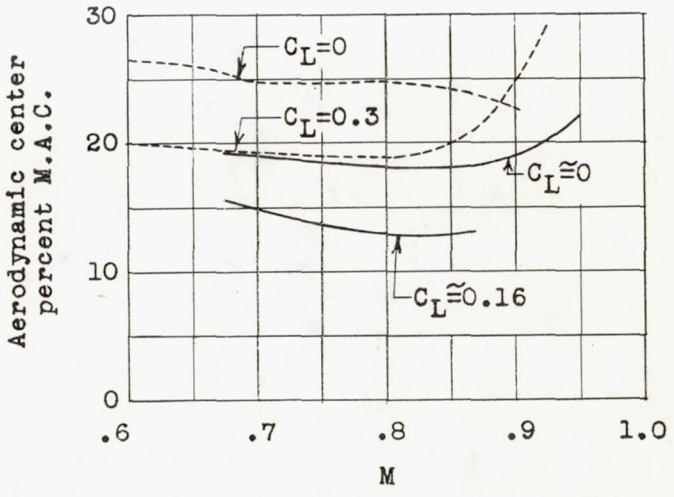

(b) Aerodynamic-center location.

⊙——Rocket model tests
---Wind tunnel tests

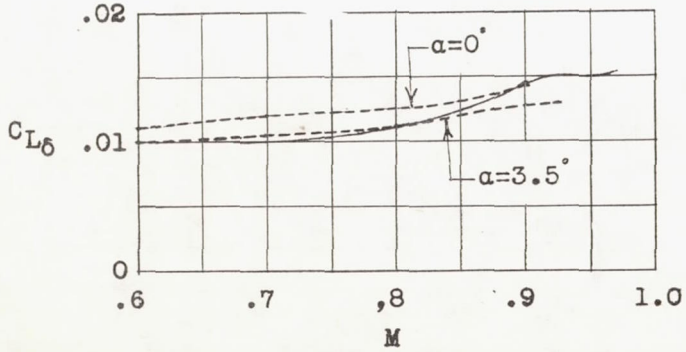

(c) Horizontal-tail effectiveness.

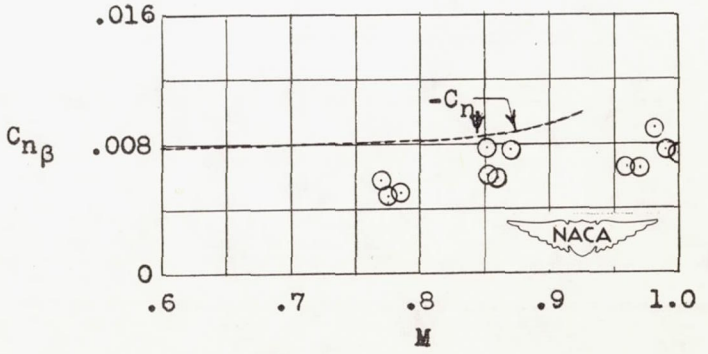

(d) Directional stability parameter.

Figure 17.- Comparisons of rocket-model and wind-tunnel data.